Energy & Environmental Science

Accepted Manuscript

ROYAL SOCIETY OF CHEMISTRY

www.rsc.org/ees

Graphics for Contents

Retarding the crystallization of PbI_2 for highly reproducible planar-structured perovskite solar cells via sequential deposition

Yongzhen Wu,[a] Ashraful Islam[a], Xudong Yang,[a] Chuanjiang Qin,[a] Jian Liu,[a] Kun Zhang,[a] Wenqin Peng[a] and Liyuan Han*[a, b]*

An universally useful idea for preparing high quality perovskite films is proposed by retarding the crystallization of PbI_2, which enabling highly reproducible planar structured perovskite solar cells.

Cite this: DOI: 10.1039/c0xx00000x

www.rsc.org/xxxxxx

ARTICLE TYPE

Retarding the crystallization of PbI_2 for highly reproducible planar-structured perovskite solar cells via sequential deposition

Yongzhen Wu,[a] Ashraful Islam[a], Xudong Yang,*[a] Chuanjiang Qin,[a] Jian Liu,[a] Kun Zhang,[a] Wenqin Peng[a] and Liyuan Han*[a, b]

Received (in XXX, XXX) Xth XXXXXXXXX 20XX, Accepted Xth XXXXXXXXX 20XX
DOI: 10.1039/b000000x

On planar substrate, sequential deposition of $CH_3NH_3PbI_3$ perovskite is optimized by retarding the crystallization of PbI_2. This strategy overcomes the problem of incomplete conversion and uncontrolled particle sizes of perovskite in absence of mesoporous scaffolds, greatly increasing the film reproducibility. Highly efficient and reproducible planar-structured perovskite solar cells were obtained with the best efficiency of 13.5%, average efficiency of 12.5% and a small standard deviation of 0.57 from totally 120 cells.

Organic-inorganic hybrid perovskite materials have gained much attention in the past years because of their high efficiency, low cost, and the ease to make these materials solution processable.[1-4] Organo-lead iodide perovskites such as $CH_3NH_3PbI_3$ have been applied in solid state mesoscopic solar cells where they were found to act not only as a light harvest, but also as an electron and hole conductor.[5-10] The ambipolar semiconducting nature of the perovskite enabled feasible construction of planar device architectures,[11-13] which simplifies their fabrication and is easier to construct flexible[14, 15] and tandem solar cells. Planar-structured devices based vapour deposited perovskite films have achieved high efficiency of 12-15%.[11, 16] However, vapour deposition will greatly increase the cost of large scale fabrication with respect to the cost-effective solution process.

Two-step sequential deposition of perovskite provides an efficient low-cost route to high performance perovskite solar cells. It was firstly applied in mesoscopic-structured substrates,[17, 18] and soon after spread to planar substrates such as ZnO,[19] TiO_2[20] as well as PSS: PEDOT,[15] enabling successful construction of several kinds of planar-structured solar cells. However, two problems were found for sequential deposition on planar substrate: one is incomplete conversion of PbI_2 and the other is uncontrolled perovskite crystal sizes as well as surface morphology.[12, 17] Full conversion of a 200 nm thick PbI_2 film to $CH_3NH_3PbI_3$ perovskite requires 2-3 h, which leads to dissolution and/or peel-off of the perovskite film into the solution.[21] Short time (seconds to tens of minutes) dipping of PbI_2 in CH_3NH_3I solution only converts part of PbI_2 and results in a $CH_3NH_3PbI_3$-PbI_2 mixture, which seems not bad to the cell efficiency[20] but not good to the devices reproducibility because the relative proportion of $CH_3NH_3PbI_3$-to-PbI_2 will be inconstant from batch to batch. On the other hand, the crystal sizes of perovskite on planar substrate without mesoporous scaffold are difficult to control, which is also unfavourable to device reproducibility. A large deviation of device performance will limit the in-depth study for further improvements. Therefore, it still needs optimization of sequential deposition on flat substrate for highly reproducible planar-structured solar cells.

Back to the two problems mentioned above, we found that both of them were caused by the easy crystallization of PbI_2, which generated different sizes of PbI_2 crystals on the substrate. On one hand, large crystals of PbI_2 greatly decrease the accessibility of organic ammonium iodide to inner lead sites, resulting in incomplete conversion. On the other hand, different sizes of PbI_2 crystals directly lead to different sizes of perovskite and uncontrolled morphology. Bearing this in mind, we considered that inhibiting the crystallization of PbI_2 may be beneficial to realize full conversion and control particle sizes of sequentially deposited perovskite. Here, we use a strong coordinative solvent of dimethylsulfoxide (DMSO) instead of commonly used N,N-dimethylmethanamide (DMF) to dissolve PbI_2 and fabricate PbI_2 films. The coordination between PbI_2 and solvent molecules, such as DMSO and DMF has been well studied in literatures.[22, 23] The coordination ratio between Pb and solvent is 1:1 and 1:2 for DMF and DMSO, with Pb-O bond length of 2.431 Å and 2.386 Å, respectively, indicating that DMSO has stronger coordination ability with PbI_2 than that of DMF. The strong interaction between DMSO and Pb^{2+} can retard the crystallization of PbI_2 as illustrated in Scheme 1, resulting in a uniform PbI_2 film showing amorphous character. When used in sequential deposition, such films can efficiently generate perovskite crystals with a full conversion within 10 min. Moreover, the resultant perovskite showed a small distribution of perovskite particle sizes at 200± 20 nm. Planar-structured solar cells combining this perovskite film with atomic layer deposited (ALD) TiO_2[24] and spiro-OMeTAD as electron- and hole-selective contacts yielded the highest efficiency of 13.5%, average efficiency of 12.5% and a very small standard deviation of 0.57 from totally 120 cells, exhibiting quite a high reproducibility.

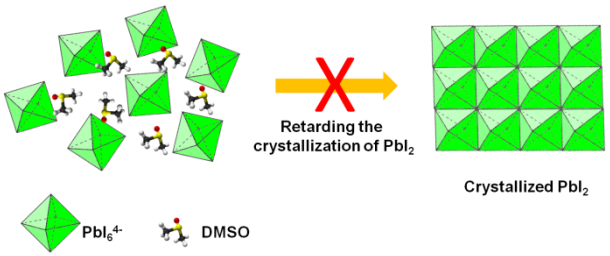

Scheme 1 Retarding the crystallization of PbI_2 by using a strongly coordinated solvent of DMSO.

The dissolution of inorganic PbI_2 in organic solvent relies on the coordination between Pb^{2+} and the electronegative atoms (such as oxygen) of the solvent molecules. Several kinds of polar solvents that contain electronegative oxygen atoms, such as DMF, dimethylacetamide, DMSO and γ-butyrolactone, showed solubility to PbI_2 in different extents. In a preliminary examination, we found that DMSO has the largest solubility (>2 M at room temperature) among these solvents, further indicating strong coordination of sulfoxide oxygen with Pb^{2+}.[25] On the other hand, DMSO has a low volatility due to its relatively high boiling point (189 °C) and low saturated vapour pressure (0.76 kPa at 60 °C), which should be benefit to maintain solvent-PbI_2 complexes stable in the films and inhibit PbI_2 crystallization in a long time scale. Therefore, DMSO was selected to fabricate PbI_2 films and compared to commonly used DMF ones.

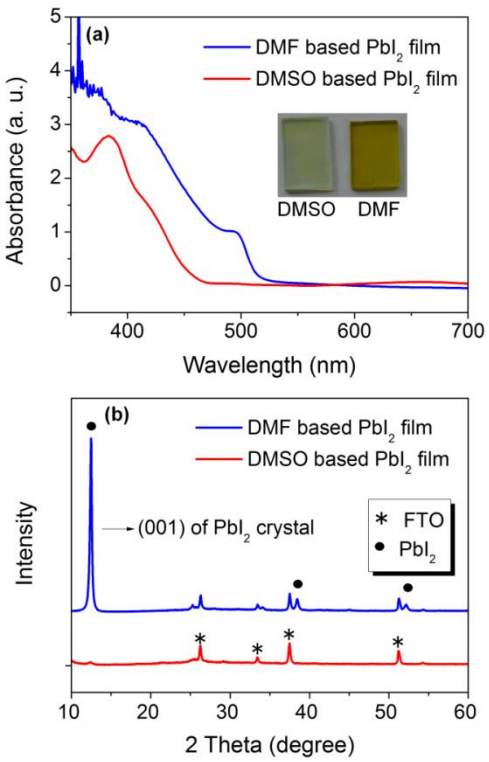

Fig. 1 UV-vis absorption spectra (a) and XRD patterns (b) of DMF and DMSO based PbI_2 films. Insert in (a) is the photo of the films.

PbI_2 films were prepared on compact TiO_2 substrate by spin-coating a solution containing 1 M PbI_2 in DMF or DMSO. Their colour is apparently different as they have different absorption spectra (Fig. 1a). DMF based PbI_2 film is featured with an absorption peak at around 500 nm, which is the characteristic band-gap excitation of crystallized PbI_2 semiconductors. While DMSO based PbI_2 film does not exhibit such absorption band, preliminary evidence of uncrystallized PbI_2. Fig. 1b shows the XRD pattern of both PbI_2 films. DMF based PbI_2 film shows a strong diffraction peak at 12.6°, corresponding to the 001 lattice plane of crystallized PbI_2. However, this characteristic diffraction peak is not present in the DMSO based PbI_2 film, further indicating its amorphous feature. We considered that such amorphous character was attributed to the stable PbI_2-DMSO complexes within the PbI_2 film, which effectively inhibited PbI_2 crystals formation as proposed in Scheme 1. Through a simple weighting experiment (ESI), we estimated that the molar ratio between PbI_2 and DMSO in the film is 1:5~6. It is not true that one Pb atom can coordinate with 5-6 DMSO molecules. As mentioned above, the coordination ratio between Pb and DMSO is 1:2. We considered that there are both coordinated and uncoordinated DMSO molecules in the film. Such a system plays an important role for retarding the crystallization of PbI_2, and enabling an amorphous feature of the film. This amorphous film could be stored for several months at room temperature. Note that if heating the film at 120 °C under vacuum for 2 h, it recovered as crystallized PbI_2 and showed similar XRD and absorption spectrum to those of DMF based PbI_2 film (Fig. S1 in ESI†).

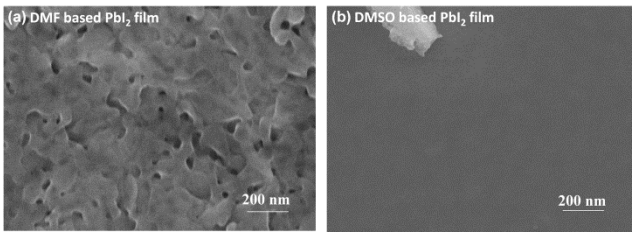

Fig. 2 SEM images of the DMF based PbI_2 films (a), DMSO based PbI_2 film (b). The dust in (b) indicates good focus of the electron beam.

Fig. 2 compares the surface morphology of DMF and DMSO based PbI_2 films. In DMF case, PbI_2 was found to form layered crystals with sizes of tens to several hundred nanometres. In contrast, the DMSO based PbI_2 film had a much more uniform surface due to its amorphous character. As we know that the crystallized PbI_2 can react with CH_3NH_3I efficiently as the ordered crystal structure already exists; only requiring the intercalation of CH_3NH_3I into the lattice to form $CH_3NH_3PbI_3$. However, the conversion of amorphous PbI_2 to ordered perovsite crystals has not been reported. Intriguingly, we found that the faint yellow DMSO based PbI_2 film can turn to dark red quickly upon dipping the film into CH_3NH_3I solution, indicating that uncrystallized PbI_2 can also generate perovskite crystals. This may be attributed to that CH_3NH_3I has a stronger binding capacity than DMSO molecules with Pb^{2+} and the former can substitute the latter to self-assembly perovskite crystals. In the following, we examined the dynamics of perovskite formation from the DMF and DMSO based PbI_2 films by optical absorption.

Fig. 3a shows the evolution of the absorbance at 750 nm (corresponding to the amount of perovskite) versus dipping time for both kinds of PbI_2 films. We can see that the crystallized PbI_2 in DMF based films indeed react very fast with CH_3NH_3I and the absorbance quickly increased from 0 to 0.4 upon dipping for 1 min. Prolonging the dipping time only slowly increased the absorbance until 40 min and after that it decreased in some

extents. This can be rationalized that PbI_2 at crystal surface can completely react with CH_3NH_3I within 1 min (Fig. S2 in ESI†), while converting the inner PbI_2 to perovskite needs quite a long time. The decrease of absorbance after 40 min is caused by perovskite peel-off as black particles can be found in the solution after long time dipping. Both the incomplete conversion and perovskite peel-off will limit its application in future reproducible devices. For DMSO based PbI_2 film, it reacted not as fast as DMF-PbI_2 in first 1 min that absorbance only increased to 0.3 at that time. However, the absorbance continuously increased until dipping for 10 min, and then it slowly decreased upon further extending dipping time. The reason for the relatively slower conversion in the first 1 min may be that CH_3NH_3I need to drive away the DMSO molecules on Pb^{2+} before the perovskite crystals could be formed. This will slow down the reaction dynamic in some extent. The continuous growth of absorbance in the first 10 min indicate that all the Pb^{2+} in the amorphous film has almost equal probability to react with CH_3NH_3I. Fig. 3b compares the XRD patterns of both kinds of films after dipping for 10 min. Note that these film were rinsed with 2-propanol and dried at 70 ^oC for 15 min before XRD characterization, which could remove the residual solvent (DMSO) if it exists (Fig. S3 in ESI†). DMSO-PbI_2 based sample (red line) only showed a set of diffraction peaks of tetragonal structured perovskite at 14.08°, 28.5°, and 31.8°. For DMF based sample, the PbI_2 diffraction (2θ = 12.6°) still exists in addition to perovsite diffractions, indicative of an incomplete conversion. Here, we emphasized that full conversion is crucial to the reproducibility of device performance because the amount of PbI_2 is uncontrollable if it exists. The relative proportions of $CH_3NH_3PbI_3$-to-PbI_2 are inconstant from batch to batch, which increases variable factors to the reproducibility of solar cell devices.

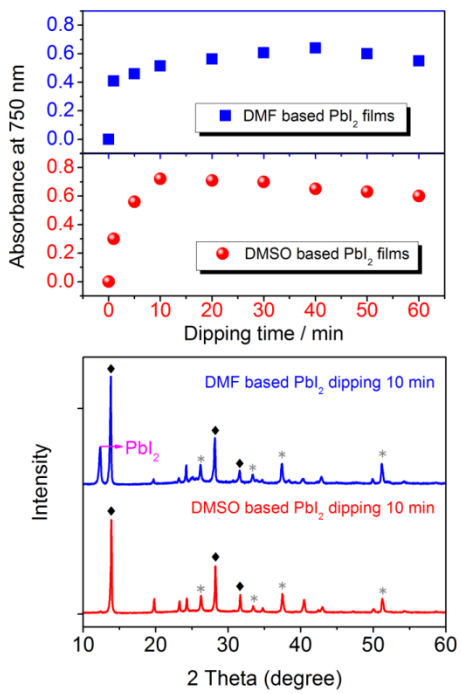

Fig. 3 (a) evolution of absorbance at 750 nm upon dipping time of the PbI_2 films in CH_3NH_3I solutions; (b) XRD patterns of the films obtained by dipping DMF and DMFO based PbI_2 films in CH_3NH_3I solutions for 10 min, * are signals come from substrate.

Except for the remaining PbI_2, morphology of perovskite film is another factor that affects the reproducibility of device performance. Fig. 4a-b show the SEM images of perovskite films obtained from DMF and DMSO based PbI_2 film, respectively. The sizes of the perovskite crystals obtained from DMF based PbI_2 film were discretely distributed, which was analysed by software (Nano Measure) as shown in Fig. 4c. The particle sizes are broadly distributed from 50 to 330 nm. This is in agreement with the size distribution of the PbI_2 crystals in the DMF based PbI_2 films. In contrast, the perovskite crystals formed from DMSO based PbI_2 film has a smaller distribution, with more than 80% located in a small range around 200 ±20 nm (Fig. 4d). This should be attributed to the controlled reaction dynamic and equal reaction probability of DMSO-PbI_2 with CH_3NH_3I. Such morphology of perovskite film with relatively uniform distribution of crystal sizes was expected to be beneficial to device reproducibility.

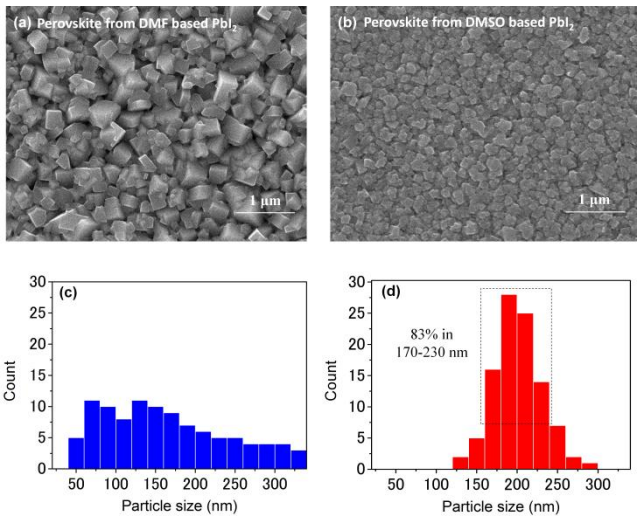

Fig. 4 SEM images of perovskite obtained from DMF (a) and DMSO (b) based PbI2 films, (c) and (d): the analysis of the particle size distribution.

Two groups (A and B, 120 cells for each group) of planar-structured perovskite solar cells were constructed with assemblies of glass/FTO/compact TiO_2/$CH_3NH_3PbI_3$/spiro-OMeTAD/Au. The $CH_3NH_3PbI_3$ perovskites in group A and group B were prepared from DMSO and DMF based PbI_2 films, respectively. The compact TiO_2 layer in solar cell device is made by atomic layered deposition, which we have proved to be beneficial to device performance and reproducibility.[24] The detailed fabrication procedure is described in ESI†. Fig. 5a shows the SEM cross-section of a complete cell taken from group A. Clearly, it has a planar structure that poly-crystalline perovskite layer was sandwiched between the compact TiO_2 layer and spiro-OMeTAD base HTM layer. Fig. 5b shows the current density–voltage (*J*–*V*) curves of the best cell in group A. It exhibited a high J_{SC} (short circuit current density) of 20.71 mA cm^{-2}, an open circuit voltage (V_{OC}) of 1.02 V and a *FF* of 0.64, resulting in a power conversion efficiency of 13.5% under standard AM 1.5 sunlight. More importantly, 87% of the cells showed efficiency greater than 12%. For devices in group B, part of them can generate high efficiencies even up to 14% but efficiency below 9% appeared frequently even prepared under same procedure. The efficiency distributions of both groups of devices are shown in

Fig. 5c and summarized in Table 1. The average efficiency of group A (12.5%) is much higher than that of group B (9.7%), and the standard deviation of efficiency for group A (0.57) is significantly lower than that group B (2.47), both of which reveal that reproducibility of group A is greatly improved with respect to group B. In consideration of the same TiO_2 and HTM layers used for the two groups of devices, the improved average efficiency and reproducibility of group A should be attributed to the optimized perovskite layer that fully converted perovskite with mean distributed crystal size can been maintained in different individual cells. As reported by H. J. Snaith and co-authors that planar-structured perovskite cells often give hysteresis in I-V curve measurement.[26] In our research, DMSO-based and DMF-based perovskite solar cells showed similar degree of hysteresis with a difference of 2-3% in the efficiency between forward scan and reversed scan. Now, the reason for the hysteresis is still not very clear and the study on hysteresis is still undergoing in our group.

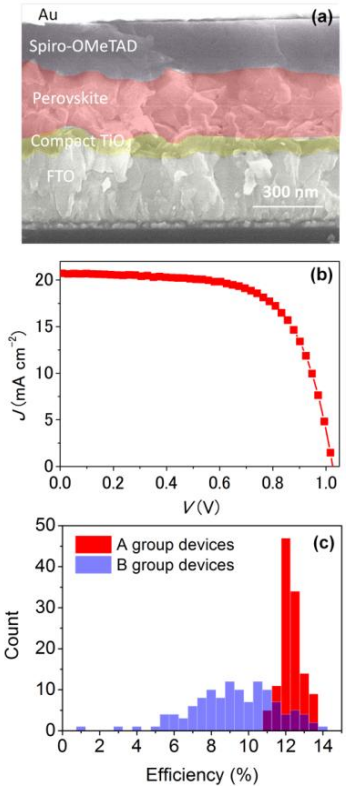

Fig. 5 (a) SEM cross-section image of an assembled device; (b) *J–V* curve of the best performing cells in group A; (c) distribution of the efficiencies from group A and B.

Table 1 Statistics of device performance in group A and B.

	Group A	Group B
The highest efficiency	13.5%	14.2%
The lowest efficiency	10.8%	1.3%
The average efficiency	12.5%	9.7%
The standard deviation	0.57	2.47

[a] The data were analyzed from totally 120 cells for each group.

Conclusions

In summary, by inhibiting the crystallization PbI_2, we have successfully prepared highly reproducible perovskite films on planar substrate via sequential deposition method. Strong coordinative DMSO instead of DMF as the solvent for PbI_2 resulted in extremely uniform and amorphous featured PbI_2 films, which were fully converted to $CH_3NH_3PbI_3$ perovskite crystals within 10 min. The resultant perovskite films showed a small distribution of crystal size and flat surface morphology. The highly reproducible perovskite films enabled reproducible planar-structured perovskite solar cells with the best efficiency of 13.5%, average efficiency of 12.5% and a small standard deviation of 0.57 from 120 specimens. The reproducible high performance devices provide platform for in-depth device studies and further optimization of photovoltaic performance. Moreover, the strategy of retarding the crystallization of precursor films worth further study and can be applied to fabricating new perovskite as well as other planar substrates.

Acknowledgments

This work was supported by grants from Core Research for Evolutional Science and Technology (CREST) of the Japanese Science and Technology Agency.

Notes and references

[a] *Photovoltaic Materials Unit, National Institute for Materials Science, Tsukuba,Ibaraki 305-0047, Japan. E-mail:YANG.Xudong@nims.go.jp, HAN.liyuan@nims.go.jp; Fax: +81 298592304; Tel:+81 298592747*
[b] *State Key Laboratory of Metal Matrix Composites, Shanghai Jiao Tong University, 800 Dong Chuan Rd. Minhang District, Shanghai 200240, China*
†Electronic Supplementary Information (ESI) available: [Experimental, SEM and XRD characterizations]. See DOI: 10.1039/b000000x/

1. A. Kojima, K. Teshima, Y. Shirai and T. Miyasaka, *J. Am. Chem. Soc.*, 2009, **131**, 6050-6051.
2. B. Cai, Y. Xing, Z. Yang, W. Zhang and J. Qiu, *Energy Environ. Sci.*, 2013, **6**, 1480-1485.
3. N. Mohammad K., P. Gao and M. Grätzel, *Energy Environ. Sci.*, 2014. DOI: 10.1039/C4EE00942H
4. T. Baikie, Y. Fang, J. M. Kadro, M. Schreyer, F. Wei, S. G. Mhaisalkar, M. Grätzel and T. J. White, *J. Mater. Chem. A*, 2013, **1**, 5628-5641.
5. H. Kim, C. Lee, J. Im, K. Lee, T. Moehl, A. Marchioro, S. Moon, R. Humphry-Baker, J. Yum, J. E. Moser, M. Grätzel and N. Park, *Sci. Rep.*, 2012, **2**.591.
6. M. M. Lee, J. Teuscher, T. Miyasaka, T. N. Murakami and H. J. Snaith, *Science*, 2012, **338**, 643-647.
7. L. Etgar, P. Gao, Z. Xue, Q. Peng, A. K. Chandiran, B. Liu, M. K. Nazeeruddin and M. Grätzel, *J. Am. Chem. Soc.*, 2012, **134**, 17396-17399.
8. J. M. Ball, M. M. Lee, A. Hey and H. J. Snaith, *Energy Environ. Sci.*, 2013, **6**, 1739-1743.
9. W. A. Laban and L. Etgar, *Energy Environ. Sci.*, 2013, **6**, 3249-3253.
10. J. H. Heo, S. H. Im, J. H. Noh, T. N. Mandal, C. Lim, J. A. Chang, Y. H. Lee, H. Kim, A. Sarkar, K. NazeeruddinMd., M. Grätzel and S. I. Seok, *Nat. Photonics*, 2013, **7**, 486-491.
11. M. Liu, M. B. Johnston and H. J. Snaith, *Nature*, 2013, **501**, 395-398.
12. Q. Chen, H. Zhou, Z. Hong, S. Luo, H. Duan, H. Wang, Y. Liu, G. Li and Y. Yang, *J. Am. Chem. Soc.*, 2013, **136**, 622-625.
13. G. E. Eperon, V. M. Burlakov, P. Docampo, A. Goriely and H. J. Snaith, *Adv. Funct. Mater.*, 2014, **24**, 151-157.
14. J. You, Z. Hong, Y. M. Yang, Q. Chen, M. Cai, T. Song, C. Chen, S. Lu, Y. Liu, H. Zhou and Y. Yang, *ACS Nano*, 2014, **8**, 1674-1680.
15. S. Sun, T. Salim, N. Mathews, M. Duchamp, C. Boothroyd, G. Xing, T. C. Sum and Y. M. Lam, *Energy Environ. Sci.*, 2014, **7**, 399-407.

16. O. Malinkiewicz, A. Yella, Y. H. Lee, G. M. Espallargas, M. Grätzel, M. K. Nazeeruddin and H. J. Bolink, *Nat. Photonics*, 2013, **8**, 128-132.
17. J. Burschka, N. Pellet, S. Moon, R. Humphry-Baker, P. Gao, M. K. Nazeeruddin and M. Grätzel, *Nature*, 2013, **499**, 316-319.
18. S. Dharani, H. K. Mulmudi, N. Yantara, P. T. Thu Trang, N. G. Park, M. Grätzel, S. Mhaisalkar, N. Mathews and P. P. Boix, *Nanoscale*, 2014, **6**, 1675-1679.
19. D. Liu and T. L. Kelly, *Nat. Photonics*, 2014, 8, 133-138.
20. A. Yella, L. Heiniger, P. Gao, M. K. Nazeeruddin and M. Grätzel, Nano Lett., 2014. **14**, 2591–2596.
21. K. Liang, D. B. Mitzi and M. T. Prikas, *Chem. Mater.*, 1998, **10**, 403-411.
22. H. Miyamae, Y. Numahata and M. Nagata, *Chem. Lett.*, 1980, **9**, 663-664.
23. A. Wakamiya, M. Endo, T. Sasamori, N. Tokitoh, Y. Ogomi, S. Hayase and Y. Murata, *Chem. Lett.*, 2014, **43**, 711-713.
24. W. A. X. Y. Yongzhen, *Appl. Phys. Express*, 2014, **7**, 52301.
25. B. Conings, L. Baeten, C. De Dobbelaere, J. D'Haen, J. Manca and H. Boyen, *Adv. Mater.*, 2013, **26**, 2041-2046.
26. H. J. Snaith, A. Abate, J. M. Ball, G. E. Eperon, T. Leijtens, N. K. Noel, S. D. Stranks, J. T. Wang, K. Wojciechowski and W. Zhang, *J. Phys. Chem. Lett.*, 2014, **5**, 1511-1515.